Simulation Modelling Practice and Theory 18 (2010) 1365–1381

Contents lists available at ScienceDirect

Simulation Modelling Practice and Theory

journal homepage: www.elsevier.com/locate/simpat

Modeling and control of the doubly fed induction generator wind turbine

Adrià Junyent-Ferré [a,*], Oriol Gomis-Bellmunt [a,c,1,2], Andreas Sumper [b,3], Marc Sala [d,4], Montserrat Mata [d,4]

[a] Centre d'Innovació en Convertidors Estàtics i Accionaments (CITCEA-UPC), E.T.S. Enginyeria Industrial Barcelona, Universitat Politècnica Catalunya, Diagonal, 647, Pl. 2, 08028 Barcelona, Spain
[b] Centre d'Innovació en Convertidors, Estàtics i Accionaments (CITCEA-UPC), E.U. Enginyeria Tècnica Industrial Barcelona, Universitat Politècnica Catalunya, Comte d'Urgell, 187, 08036 Barcelona, Spain
[c] IREC Catalonia Institute for Energy Research, Josep Pla, B2, Pl. Baixa, 08019 Barcelona, Spain
[d] Alstom Wind Power, Roc Boronat, 78, 08005 Barcelona, Spain

ARTICLE INFO

Article history:
Received 18 November 2009
Received in revised form 29 April 2010
Accepted 30 May 2010
Available online 4 June 2010

Keywords:
Doubly fed induction machine
Wind turbine power generation
Vector control
Simulation

ABSTRACT

The present paper deals with the modeling of wind turbine generation systems. The model of a doubly fed induction generator, along with the corresponding converter, crow bar protection and electrical grid is described. The different level control strategies both in normal operation and under voltage dig conditions are discussed, including speed control, torque and reactive power control for the rotor-side converter, reactive and DC voltage control for the grid-side converter and the corresponding current loops control. The results obtained with simulations are compared to experimental data obtained from voltage sags provoked to real wind turbines.

1. Introduction

Wind power may be considered as one of the most promising renewable energy sources after its progress during the last three decades. However, its integration into power systems has a number of technical challenges concerning security of supply, in terms of reliability, availability and power quality. Wind power impact mainly depends on its penetration level, but depends also on the power system size, the mix of generation capacity, the degree of interconnections to other systems and load variations. Since the penetration of wind power generation is growing, system operators have an increasing interest in analyzing the impact of wind power on the connected power system. For this reason, grid connection requirements are established. In the last few years, the connection requirements have incorporated, in addition to steady state problems, dynamic requirements, like voltage dip ride-through capability. This leads to the need for detailed modeling of wind turbine systems in order to analyze the dynamic phenomena in the power grid.

Moreover, new wind turbine technology integrates power electronics and control making it possible for wind power generation to participate in active and reactive power control. The typical generator configuration for new variable speed turbine is the doubly fed induction generator (DFIG) shown in Fig. 1. This configuration consists of a wound rotor induction generator where the stator windings are directly connected to the grid and the rotor windings connected to a back-to-back

* Corresponding author. Tel.: +34 934054246.
E-mail address: adria.junyent@citcea.upc.edu (A. Junyent-Ferré).
[1] Tel.: +34 934054246.
[2] Tel.: +34 93 3562615.
[3] Tel.: +34 934037432.
[4] Tel.: +34 932257600.

1569-190X/$ - see front matter © 2010 Elsevier B.V. All rights reserved.
doi:10.1016/j.simpat.2010.05.018

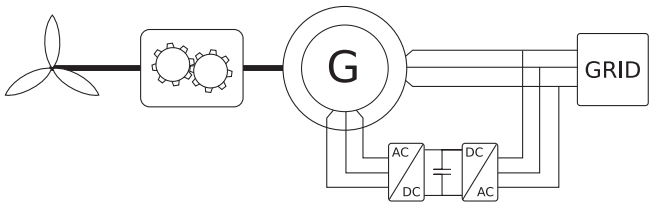

Fig. 1. Variable speed wind turbine scheme.

power converter. This back-to-back power converter is dimensioned for partial generator power and is able to operate bi-directionally.

The massive employment of DFIG machines has lead to motivate the modeling [1] of such doubly fed induction generators, mainly in the issues related to power quality and ride-through capability. Different modeling approaches are presented in [2,3] for grid integration studies. A doubly fed induction generator model for transient stability analysis is proposed in [4], considering the control loops of instantaneous response. In [5–7] the ride-through capability of doubly fed induction generators is studied. The response under unbalanced sags is addressed in [8,9]. A DFIG ride-through control scheme without crow bar is suggested in [10]. As far as the converter control is concerned, some proposals have been added to classical approach of [11,12], sliding mode control is used in [13]. The power control of a doubly fed induction machine via output feedback is investigated in [14,15]. A model reference adaptive system (MRAS) observer for sensorless control of standalone doubly fed induction generators is addressed in [16]. The behaviour of such machines in large wind farms, along with the general reactive and active power control of wind farms have been studied in [17,18].

Due to the large dimensions of the wind turbines, usually small scale laboratory prototypes are used to validate the simulation models meant for large wind turbines. The present work presents a model focussed in the proper simulation of the wind turbine behavior and compares the simulation results obtained from the developed model with real measurements from a real test done in a full scale 1.5 MW wind turbine from Alstom.

The model formulation for the induction generator, the back to back converter (including the crow bar) and the electrical network is presented. Also the detailed description of the reactive power, DC bus voltage and torque controllers, along with its corresponding current loops. Simulation results are analyzed and discussed.

The paper has been structured as follows. In Section 2 the modelization of the system is discussed. The control scheme is presented in Section 3. The model validation is presented in Section 4, showing the comparison of results from simulations and from real voltage sags. Finally, the conclusions are summarized in Section 5.

2. Model

2.1. Wind wheel modeling

Wind turbine electrical generation systems' (WTGS) power comes from the kinetic energy of the wind, thus it can be expressed as the kinetic power available in the stream of air multiplied by a C_P factor called power coefficient or Betz's factor. C_P mainly depends on the relation between the average speed of the air across the area covered by the wind wheel and its angular speed and geometric characteristics of the turbine (including the instantaneous blade pitch angle configuration)[19]. The power extracted by the wind turbine has the following expression:

$$P_{ww} = c_P P_{\text{wind}} = c_P \frac{1}{2} \rho A v_w^3, \tag{1}$$

where P_{wind} is the air stream kinetic power, ρ is the air density assumed to be constant, A is the surface covered by the wind wheel and v_w is the average wind speed.

There have been different approaches to model the power coefficient ranging from considering it to be constant for steady state and small signal response simulations to using lookup tables with measured data. Another common approach is to use an analytic expression originated from [19] of the form:

$$c_P(\lambda, \theta_{\text{pitch}}) = c_1 \left(c_2 \frac{1}{\Lambda} - c_3 \theta_{\text{pitch}} - c_4 \theta_{\text{pitch}}^{c_5} - c_6 \right) e^{-c_7 \frac{1}{\Lambda}}, \tag{2}$$

where λ is the so called tip-speed ratio and it is defined as

$$\lambda = \frac{\omega_t R}{v_w}, \tag{3}$$

where ω_t is the turbine speed, R is the turbine radius and Λ is defined as

$$\frac{1}{\Lambda} = \frac{1}{\lambda + c_8 \theta_{\text{pitch}}} - \frac{c_9}{1 + \theta_{\text{pitch}}^3}, \tag{4}$$

where $[c_1,\ldots,c_9]$ are characteristic constants for each wind turbine and θ_{pitch} is the blade pitch angle.

Thus by knowing the wind speed, the angular speed of the wind turbine and the blade pitch angle, the mechanical torque on the turbine shaft can be easily computed.

2.2. Wind speed modeling

Wind speed usually varies from one location to another and also fluctuates over the time in a stochastic way. As it has been previously seen, it maintains a direct relation to the torque over the turbine axis and therefore it may also have some direct effect on the power output of the WTGS hence its evolution must be taken into account to properly simulate the WTGS dynamics.

One possible approach to generate the wind speed signal on simulations may be to use logs of real measurements of the speed on the real location of the WTGS. This approach has some evident limitations because it requires a measurement to be done on each place to be simulated. Another choice, proposed by Slootweg [20] is to use a mathematical model which takes some landscape parameters to generate a wind speed sequence for any location. This wind speed expression has the form:

$$v_w(t) = v_{wa}(t) + v_{wr}(t) + v_{wg}(t) + v_{wt}(t), \tag{5}$$

where $v_{wa}(t)$ is a constant component, $v_{wr}(t)$ is a common ramp component, v_{wg} is a gust component and v_{wt} is a turbulence component.

The gust component may be useful to simulate an abnormal temporary increase of the speed of the wind and its expression is

$$v_{wg}(t) = \begin{cases} 0, & \text{for } t < T_{sg}, \\ \widehat{A}_g\left(1 - \cos\left[2\pi\left(\frac{t-T_{sg}}{T_{eg}-T_{sg}}\right)\right]\right), & \text{for } T_{sg} \leqslant t \leqslant T_{eg}, \\ 0, & \text{for } T_{eg} < t, \end{cases} \tag{6}$$

where $\widehat{A}_g$ is the amplitude of the gust and T_{sg} and $T_{e.g.}$ are the start and the end time of the gust.

Finally, as discussed in [21], the turbulence component is a signal which has a power spectral density of the form:

$$P_{Dt}(f) = \frac{l\hat{v}_w\left[\ln\left(\frac{h}{z_0}\right)\right]^{-2}}{\left[1 + 1.5\frac{fl}{\hat{v}_w}\right]^{5/3}}, \tag{7}$$

where $\hat{v}_w$ is the average wind speed, h is the height of interest (the wind wheel height), l is the turbulence scale which is twenty times h and has a maximum of 300 m and z_0 is a roughness length parameter which depends on the landscape type as shown in Table 1.

By knowing the height of the wind turbine, the average wind speed and the kind of landscape where the WTGS is, the power spectral density of the wind speed turbulence is known. The next step is to generate a signal, function of time, which has the desired power spectral density. There are many ways of doing this: by summing a large number of sines with random phases and amplitudes according to the P_{Dt} function as [22] or by designing a shaping filter and applying it to a flat spectrum noise signal. Provided that the P_{Dt} is very close to the response of a first order filter, the use of this kind of filter is suggested here. The designed filter's transfer equation is

$$H(s) = \frac{K}{s+p}, \tag{8}$$

with

$$p = \frac{2\pi\left(\left(K_1^2\right)^{3/5} - 1\right)}{K_2\sqrt{K_1^2 - 1}}, \quad K = K_1 p, \tag{9}$$

where K_1 and K_2 are defined as

Table 1
Values of the z_0 for different types of landscapes. *Sources*: Panofsky and Dutton, 1984; Simiu and Scanlan, 1986.

Landscape type	Range of z_0 (m)
Open sea or sand	0.0001–0.001
Snow surface	0.001–0.005
Mown grass or steppe	0.001–0.01
Long grass or rocky ground	0.04–0.1
Forests, cities and hilly areas	1–5

$$K_1 = l\hat{v}_w\left[\ln\left(\frac{h}{z_0}\right)\right]^{-2}, \tag{10}$$

$$K_2 = 1.5\frac{l}{\hat{v}_w}, \tag{11}$$

and the power spectral density of the generated signal has the form:

$$P_{\text{filter}} = \frac{\frac{K^2}{p^2}}{1+\frac{4\pi^2}{p^2f^2}}. \tag{12}$$

2.3. Drive train modeling

The drive-train of a WTGS comprises the wind wheel, the turbine shaft, the gearbox, and the generator's rotor shaft. The gearbox usually has a multiplication ratio between 50 and 150 and the wind wheel inertia usually is about the 90% of the inertia of the whole system.

Because of the high torque applied to the turbine shaft, its deformation must not be neglected and its elastic behaviour should be taken into account because of its filtering properties. A common way to model the drive-train is to treat it as a series of masses connected through an elastic coupling with a linear stiffness, a damping ratio and a multiplication ratio between them. On this paper a model with two masses, graphically presented in Fig. 2, is used treating the wind wheel as one inertia J_t and the gearbox and the generator's rotor as another inertia J_m connected through the elastic turbine shaft with a k angular stiffness coefficient and a c angular damping coefficient. Applying the Newton's laws, the dynamics of the resulting system can be described as

$$\begin{Bmatrix} \dot{\omega}_m \\ \dot{\omega}_t \\ \omega_m \\ \omega_t \end{Bmatrix} = \begin{pmatrix} \frac{-v^2c}{J_m} & \frac{vc}{J_m} & -\frac{v^2k}{J_m} & \frac{vk}{J_m} \\ \frac{vc}{J_t} & -\frac{c}{J_t} & \frac{vk}{J_t} & -\frac{k}{J_t} \\ 1 & 0 & 0 & 0 \\ 0 & 1 & 0 & 0 \end{pmatrix} \begin{Bmatrix} \omega_m \\ \omega_t \\ \theta_m \\ \theta_t \end{Bmatrix} + \begin{pmatrix} \frac{1}{J_m} & 0 \\ 0 & \frac{1}{J_t} \\ 0 & 0 \\ 0 & 0 \end{pmatrix} \begin{Bmatrix} \tau_m \\ \tau_t \end{Bmatrix}, \tag{13}$$

where θ_t and θ_m are the angles of the wind wheel and the generator shaft, ω_t and ω_m are the angular speed of the wind wheel and the generator, τ_t is the torque applied to the turbine axis by the wind wheel and τ_m is the generator torque.

2.4. Generator modeling

The generator of a doubly fed WTGS is a wounded rotor asynchronous machine. Assuming the stator and rotor windings to be placed sinusoidally and symmetrical, the magnetical saturation effects and the capacitance of all the windings neglectable and the neutral of the stator and rotor windings to be floating and taking as positive the currents flowing towards the machine, the relations between the voltages on the machine windings and the currents and its first derivative may be written on a synchronous reference qd frame representation as

$$\begin{Bmatrix} v_{sq} \\ v_{sd} \\ v_{rq} \\ v_{rd} \end{Bmatrix} = \begin{bmatrix} L_s & 0 & M & 0 \\ 0 & L_s & 0 & M \\ M & 0 & L_r & 0 \\ 0 & M & 0 & L_r \end{bmatrix} \frac{d}{dt} \begin{Bmatrix} i_{sq} \\ i_{sd} \\ i_{rq} \\ i_{rd} \end{Bmatrix} + \begin{bmatrix} r_s & L_s\omega_s & 0 & M\omega_s \\ -L_s\omega_s & r_s & -M\omega_s & 0 \\ 0 & sM\omega_s & r_r & sL_r\omega_s \\ -sM\omega_s & 0 & -sL_r\omega_s & r_r \end{bmatrix} \begin{Bmatrix} i_{sq} \\ i_{sd} \\ i_{rq} \\ i_{rd} \end{Bmatrix}, \tag{14}$$

where L_s and L_r are the stator and rotor windings self-inductance coefficient, M is the coupling coefficient between stator and rotor windings and s is the slip.

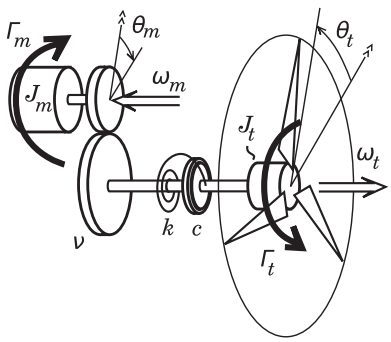

Fig. 2. Two mass drive-train model.

Also the torque expression and the stator reactive power, which are the control objectives of the rotor-side converter control, have the following form:

$$\Gamma_m = \frac{3}{2} PM(i_{sq} i_{rd} - i_{sd} i_{rq}), \tag{15}$$

and

$$Q_s = \frac{3}{2}(v_{sq} i_{sd} - v_{sd} i_{sq}), \tag{16}$$

where P is the number of pairs of poles of the generator.

When simulating the system, expression (14) is rewritten to have the current derivatives as a function of the instantaneous currents and the applied voltages as in the usual system space-state representations.

2.5. Converter modeling

The most common topology [23] of the converter of the doubly fed WTGS is the IGBT voltage source back-to-back converter with an inverter connected to the rotor windings fed by a DC bus connected to another inverter which acts as an active rectifier connected to a three phase grid through a filter inductance in a series connection (graphically represented in Fig. 3). The so-called crow bar can be connected in parallel before the converter on the rotor side or in the DC bus, it acts as an auxiliary mechanism to avoid overvoltages in the DC bus due to excessive power flowing from the rotor inverter to the grid-side converter.

Dealing with the modelization of the converter is not a trivial task and different levels of detail may be achieved doing some assumptions. In this work, it is assumed that the switching frequency is high enough to assume that the high-frequency components of the voltage signals generated by the inverters are totally filtered by the system and also that the switching energy losses can be neglected.

Making this assumptions, the dynamics of the grid-side electrical circuit between the grid voltage and the voltage applied on the AC side of the converter assuming the currents positive when flowing towards the machine can be described as

$$v_z^{abc} - v_l^{abc} - (v_{cn} - v_{zn}) \begin{Bmatrix} 1 \\ 1 \\ 1 \end{Bmatrix} = r_l i_l^{abc} + L_l \frac{d}{dt} i_l^{abc}, \tag{17}$$

and

$$v_{cn} - v_{zn} = \frac{1}{3}(v_{za} + v_{zb} + v_{zc} - v_{la} - v_{zb} - v_{zc}), \tag{18}$$

where v_z^{abc} and v_l^{abc} are the abc voltage vectors of the grid and the AC side of the converter, r_l is the resistance of the filter inductors and L_l is the inductance of the filter.

The dynamics of the voltage of the DC bus can be described as

$$E = E_0 + \frac{1}{C} \int_0^t (i_{DCl} - i_{DCr}) dt, \tag{19}$$

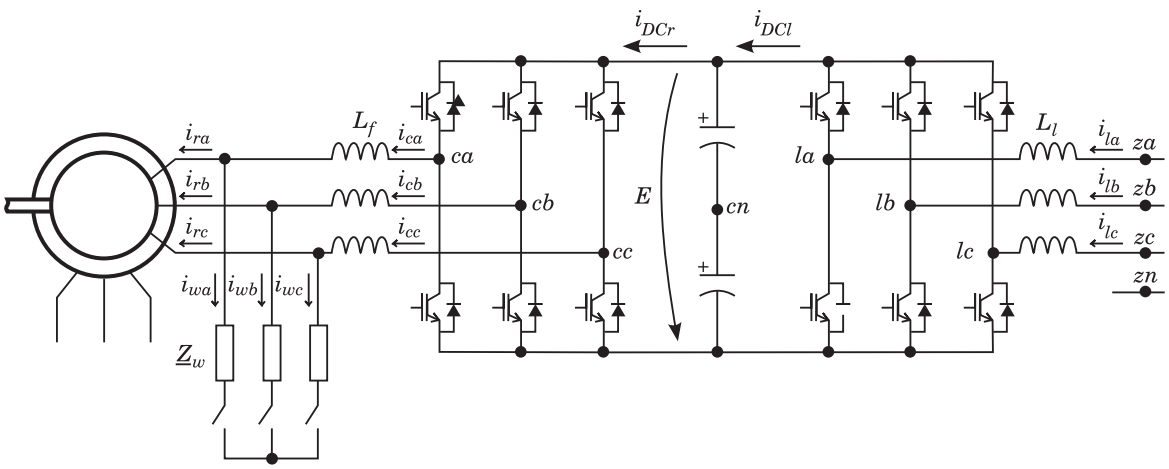

Fig. 3. The machine side and grid-side converter.

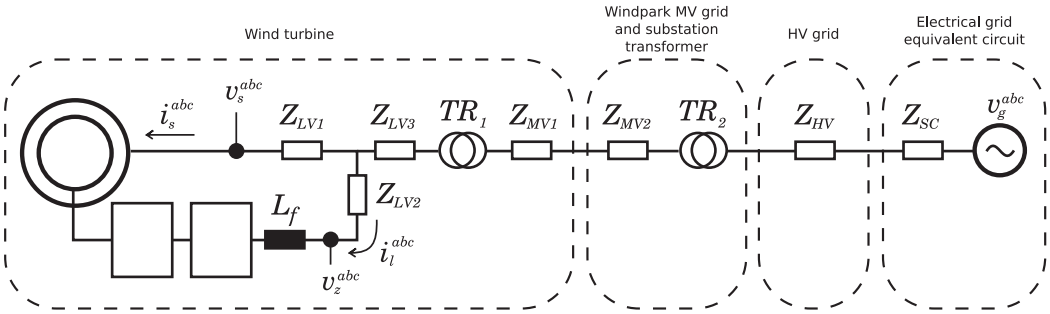

Fig. 4. The grid model.

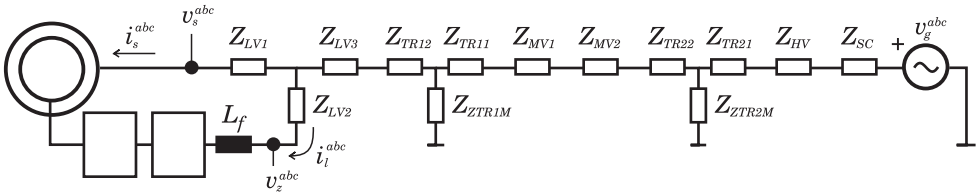

Fig. 5. The grid model's electrical circuit.

where E is the voltage of the DC bus, i_{DCl} is the current through the DC side of the grid-side inverter, i_{DCr} is the current through the DC side of the rotor-side inverter and both currents can be computed by doing a power balance on each inverter.

The crow bar is assumed to be on the AC side of the rotor converter and its applied voltages to be the same as the ones on the rotor windings generated by the rotor-side inverter (as shown in Fig. 3). Making these assumptions, the current through the AC side of the rotor converter can be described as

$$i_c^{abc} = i_r^{abc} + i_w^{abc}, \tag{20}$$

where i_c^{abc} and i_w^{abc} are the rotor converter and the crow bar *abc* current vector.

The dynamics of the current through the crow bar can be described as

$$\frac{d}{dt} i_w^{abc} = -\frac{r_w}{L_w} i_w^{abc} + \frac{1}{L_w} v_r^{abc}, \tag{21}$$

where r_w and L_w are the crow-bar resistance and inductance.

2.6. Grid modeling

The grid's model comprises from the conductors connected to the stator and rotor windings to the whole country grid (Fig. 4).

A simplified grid model consisting in a grid of impedances and an ideal three phase voltage source is used. The stator and rotor voltages are fully determined and thus can be computed from the values of the stator and rotor currents and the grid model's generator voltage. Fig. 5 depicts the electrical circuit of the model.

3. Control

The control problem of variable speed WTGSs, as many electrical actuator problems, can be split into two separate control problems with different time constants: a fast-response electrical control and a slow-response speed control. This decomposition is depicted in Fig. 6 and a block-diagram of the electrical control which will be explained in the following sections can also be seen in Fig. 7. The speed control, which may also be thought as part of a high level control, actuates on the pitch angle and gives torque signal references to the electrical control which actuates on the converter.

3.1. Speed control

There are two main modes of operation of the variable speed WTGSs: the partial load and the full load, and the speed control system acts in a different way in each one. In the partial-load region, the goal of the control system is to capture

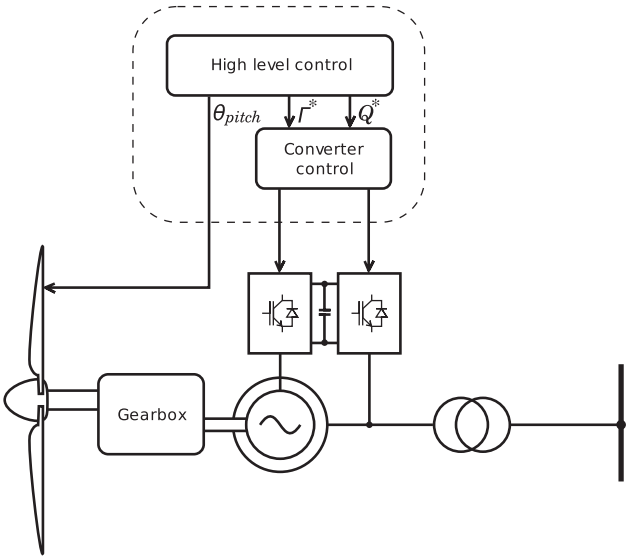

Fig. 6. The general control scheme.

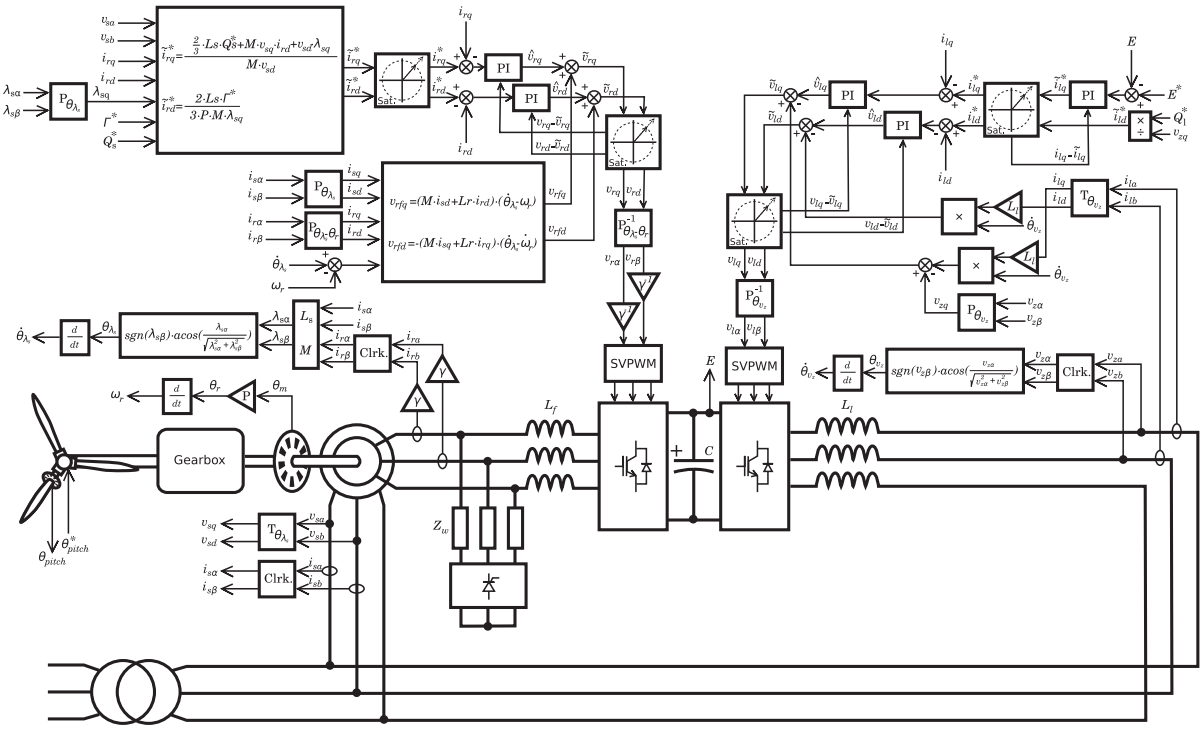

Fig. 7. The converter control diagram.

as much energy from the wind as possible while on the full load region its goal is to keep extracting the nominal power while avoiding overloads. In each region different control schemes are possible.

In the present work, only the partial-load region is considered and the constant tip-speed ratio, which is the most common partial-load scheme, is analyzed. The constant tip-speed ratio scheme leaves the pitch angle in a fixed position and gives torque references to the electrical control as a function of the rotating speed. Thus, the advantage of this scheme is that it does not require a wind speed measurement but also its main drawback is that its open-loop nature does not warrant the maximum power extraction.

To find the torque function that gives the optimal power extraction we take the C_P function and find its maximums. By doing the derivative of the expression (2) with respect to the tip-speed ratio and solving the zero, a maximum of the C_P for is found on λ_{opt} and its value is

$$C_{P\text{opt}} = c_1 c_2 c_7^{-1} e^{-\frac{c_4 c_7 \theta_{\text{pitch}}^{c_5} + c_3 c_7 \theta_{\text{pitch}} + c_6 c_7 + c_2}{c_2}}. \tag{22}$$

By substituting $C_{P\text{opt}}$ and λ_{opt} on the extracted power expression (1) and dividing it by the angular speed, a turbine torque for the maximum power extraction expression is obtained which for $\theta_{\text{pitch}} = 0$ (a common value for the pitch in the partial-load region) has the following form:

$$\Gamma_{\text{opt}}\big|_{\theta_{\text{pitch}}=0} = \frac{c_1 e^{-\frac{c_6 c_7 + c_2}{c_2}} (c_2 c_7 c_9 + c_6 c_7 + c_2)^3}{c_2^2 c_7^4} \frac{1}{2} \rho A R^3 \omega_t^2 = K_{C_P}\Big|_{\theta_{\text{pitch}}=0} \omega_t^2, \tag{23}$$

where R is the length of the blades of the wind wheel and K_{C_P} is optimal torque coefficient of the turbine.

It can easily be proven that if the pitch keeps constant and the optimal torque function is passed as reference to the electrical control, the system tends to an equilibrium point corresponding to the maximum power extraction point for each wind speed.

3.2. Rotor-side converter control

The control of the induction generator is done by the rotor-side control system by vector control using a synchronous reference with the q axis aligned to the computed stator flux. This control scheme requires the measurement of the stator and rotor currents, the stator windings voltages and the rotor angle and has the advantage that it provides a nearly decoupled control between the torque and the reactive power.

The control is divided in two stages: on a first stage, the rotor current references are computed using the following expressions which can be deduced from (15) and (16):

$$\begin{Bmatrix} \tilde{i}_{rq}^* \\ \tilde{i}_{rd}^* \end{Bmatrix} = \begin{Bmatrix} \frac{\frac{2}{3} L_s Q_s^* + M v_{sq} i_{rd} + v_{sd} \lambda_{sq}}{M v_{sd}} \\ \frac{2 L_s \Gamma_m^*}{3 P M \lambda_{sq}} \end{Bmatrix}, \tag{24}$$

where λ_{sq} is the stator flux.

These current references are then saturated of modulus according to the current limitations of the rotor-side converter and fed to the second stage of current control loops.

The control of the current is done by linearizing the current dynamics using the following state feedback:

$$\begin{Bmatrix} v_{rq} \\ v_{rd} \end{Bmatrix} = \begin{Bmatrix} \hat{v}_{rq} + M(\omega_{\lambda_s} - \omega_r) i_{sd} + L_r(\omega_{\lambda_s} - \omega_r) i_{rd} \\ \hat{v}_{rd} - M(\omega_{\lambda_s} - \omega_r) i_{sq} - L_r(\omega_{\lambda_s} - \omega_r) i_{rq} \end{Bmatrix}, \tag{25}$$

where $\hat{v}_{rq}$ and $\hat{v}_{rd}$ are the output voltages of two controllers, ω_{λ_s} is the time derivative of the phase of the stator flux and ω_r is the generator angular speed seen by the electrical system.

If the effect of the derivative of the stator current is neglected, the linearization leads to the following expression of the current dynamics where the q and d components are decoupled:

$$\frac{d}{dt} \begin{Bmatrix} i_{rq} \\ i_{rd} \end{Bmatrix} = -\begin{bmatrix} \frac{r_r}{L_r} & 0 \\ 0 & \frac{r_r}{L_r} \end{bmatrix} \begin{Bmatrix} i_{rq} \\ i_{rd} \end{Bmatrix} + \begin{bmatrix} \frac{1}{L_r} & 0 \\ 0 & \frac{1}{L_r} \end{bmatrix} \begin{Bmatrix} \hat{v}_{rq} \\ \hat{v}_{rd} \end{Bmatrix}. \tag{26}$$

Thus, the controller can be designed using any of the classical linear control techniques, in this study the Internal Model Control (IMC) [24] is used. The parameters of a proportional-integrator controller (PI) are obtained giving a desired system time constant τ (and thus desired bandwidth) using the following parameters:

$$K_p = \frac{L_r}{\tau}, \quad K_i = \frac{r_r}{\tau}. \tag{27}$$

By choosing a high bandwidth, the gain of the controller increases and the controller action becomes more likely to saturate because of the voltage limitation of the converter thus worsening the response of the system. Also it should be avoided to have a large gain at higher frequencies due to the switching nature of the converter.

3.3. Grid-side converter control

The grid-side converter controls the voltage of the DC bus and acts as an active filter which can generate reactive power. Its control is done using a synchronous reference frame with its q axis aligned to the grid voltage which allows active and reactive decoupled control and requires the measurement of the grid and DC bus voltages and the currents of the AC side of the grid converter.

To control the reactive power, a i_{ld} reference is computed from the desired grid-side reactive power and the instantaneous grid voltage as follows:

$$i_{ld}^{*} = \frac{2Q_z^{*}}{3v_{zq}}, \tag{28}$$

where Q_z^{*} is the desired grid-side reactive power.

The active power, which is responsible of the evolution of the DC bus voltage is controlled by the i_{lq} component and its reference signal is output by a linear controller designed to give a zero stationary voltage error for a constant power flow from the rotor-side converter. When designing the controller, some assumptions are done because of the non-linear dynamics involved in the evolution of the DC bus voltage as described in [11]. The dynamics of the voltage error are described by the following Laplace function:

$$e(s) = \frac{s}{s + \frac{3m}{2C}G_c(s)}E^{*}(s) + \frac{\frac{1}{C}}{s + \frac{3m}{2C}G_c(s)}i_{DCr}(s), \tag{29}$$

where m is a term which is assumed to be constant and can be computed as the grid voltage divided by the DC bus voltage, C is the capacitance of the DC bus, $E^{*}(s)$ is the Laplace transform of the desired DC bus voltage evolution (usually constant) and $G_c(s)$ is the transfer function of the controller.

Assuming the current control fast enough to consider its evolution instantaneous for the DC bus voltage control loop, the zero stationary error objective for a constant power flow from the rotor side can be obtained by using a PI controller which also gives a desired damping ratio and natural frequency by using the following PI parameters:

$$K_i = \frac{2C}{3m}\omega_n^2, \tag{30}$$

$$K_p = \frac{4C}{3m}\zeta\omega_n, \tag{31}$$

where ζ can be chosen to be greater than 1 to have a overdamped response without oscillations and ω_n can be chosen to have the desired response speed.

The computed current references are limited according to the converter capabilities and fed to the current control loops.

The grid-side current dynamics of the AC side are described by the following expression in the grid voltage q-aligned synchronous frame:

$$\begin{Bmatrix} v_{zq} \\ 0 \end{Bmatrix} - \begin{Bmatrix} v_{lq} \\ v_{ld} \end{Bmatrix} = \begin{bmatrix} r_l & -L_l\omega_e \\ L_l\omega_e & r_l \end{bmatrix}\begin{Bmatrix} i_{lq} \\ i_{ld} \end{Bmatrix} + \begin{bmatrix} L_l & 0 \\ 0 & L_l \end{bmatrix}\frac{d}{dt}\begin{Bmatrix} i_{lq} \\ i_{ld} \end{Bmatrix}. \tag{32}$$

The current control is done by the following state linearization feedback as with the rotor currents:

$$\begin{Bmatrix} v_{lq} \\ v_{ld} \end{Bmatrix} = \begin{Bmatrix} -\hat{v}_{lq} + v_{zq} - L_l\omega_e i_{lq} \\ -\hat{v}_{ld} + L_l\omega_e i_{ld} \end{Bmatrix}, \tag{33}$$

where the $\hat{v}_{lq}$ and $\hat{v}_{ld}$ are the voltages output by the current controller.

The controller is designed the same way as the current controller of the rotor side, using the methodology exposed in [24]. The parameters of a PI controller to obtain a desired time constant τ are obtained:

$$K_p = \frac{L_l}{\tau}, \quad K_i = \frac{r_l}{\tau}. \tag{34}$$

3.4. Crow bar control

The crow bar control, as mentioned before, acts when the grid-side converter is not capable of outputting the whole power coming through the DC bus from the rotor converter to avoid the overvoltage of the DC bus capacitors. Its activation is triggered for a fixed time when the DC bus voltage exceeds a high threshold and disconnects as soon as the voltage is lower than a lower threshold. During its operation, the rotor-side converter may be disconnected as described in [5] although some authors [6] suggest to keep the converter connected to avoid loosing control over the machine. In the present work the rotor-side converter is disconnected, thus suppressing the rotor converter current, allowing a fast DC bus voltage response.

3.5. Converter limits

The presence of limitations on the applicable controller actions is an important yet difficult to study subject in the analysis and design of control systems. Systematic study methodologies have been proposed to deal with actuator saturation [25] but as this is not the main subject here, another common pragmatical strategy is applied.

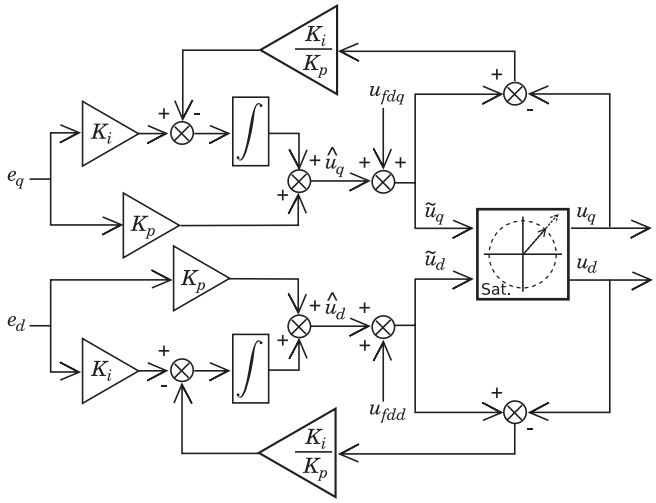

Fig. 8. The *anti-windup* modification.

First the controller system is designed neglecting the limitations of the converter and then anti-windup modifications are introduced to the control loops to avoid the undesired unlimited increase of the integral part of the PI controllers due to the saturation effect. These anti-windup modifications are depicted in Fig. 8.

4. Simulation and validation results

In order to test the matching of the model, a real voltage dip response test done on a real WTGS is simulated and its results compared to the measurements done in the test. The real test was done in the partial-load operation region on a ECO74 Wind turbine from Alstom (see Fig. 9) and measures of the electrical magnitudes on the MV-side of the TR1 transformer are available to compare with simulation results (see Fig. 10). Table 2 shows the parameters of the operating point before the voltage dip and the nominal values used to compute the per-unit (pu) quantities.

The voltage dip tested is a symmetrical gap applied to the medium voltage side of the TR1 transformer. Table 3 shows the parameters of the gap and Fig. 11 shows the root mean square (rms) graph of the measured MV voltages from the experimental test which are also used as input to the model.

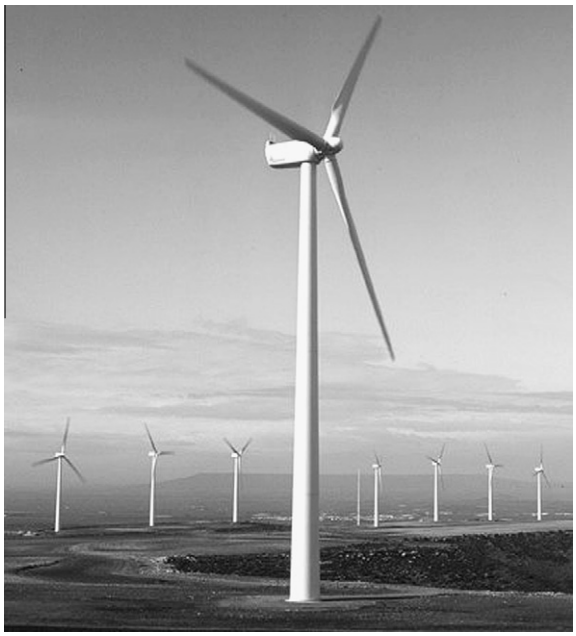

Fig. 9. Picture of a real ECO74 WTGS. More detail is available on http://www.power.alstom.com.

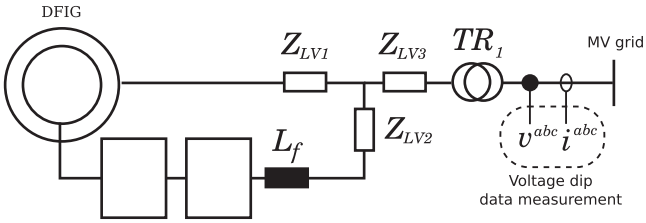

Fig. 10. Scheme of the voltage dip test measurement.

Table 2
Base and operational parameters.

Parameter	Value	Units
Nominal power (stator plus rotor)	1.76	MVA
Nominal MV voltage	17.32	kV (phase to phase rms)
Nominal MV current	33.81	A (rms)
Rotor-side converter rated power	750	kVA
Grid-side converter rated power	480	kVA
Active power before the voltage dip	0.1532	pu
Reactive power before the voltage dip	0.0033	pu

Table 3
Voltage dip parameters.

Parameter	Value	Units
Duration	540	ms
Voltage amplitude during the dip	0.215	pu
Drop start ramp length	15	ms
Drop end ramp length	30	ms

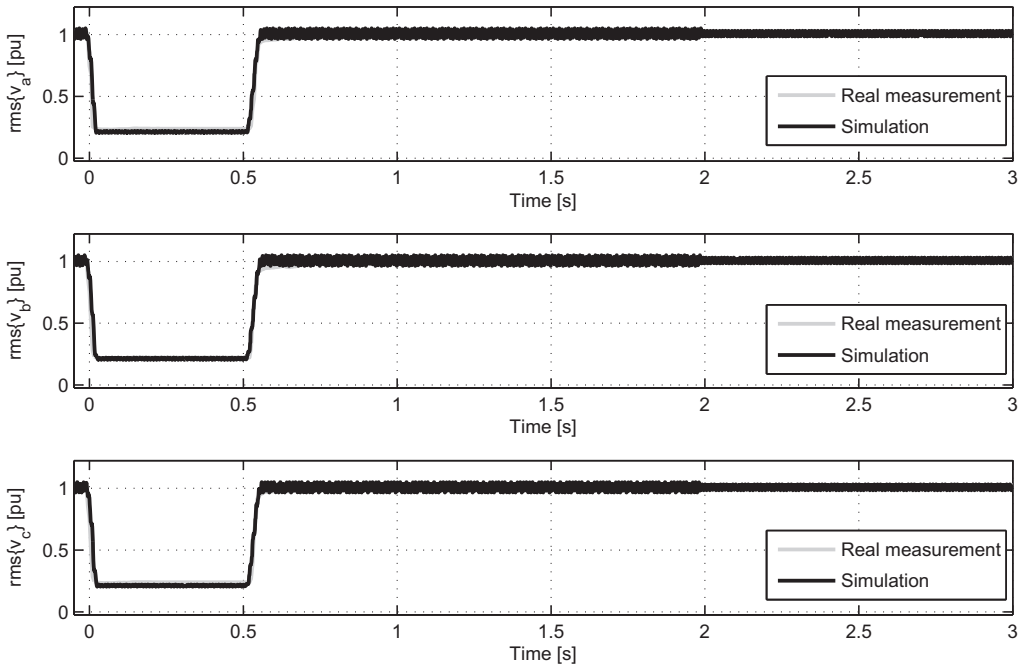

Fig. 11. RMS value of the *abc* voltages of the MV-side of the TR1 transformer.

Different strategies exist to deal with the voltage dip and avoid having to disconnect the WTGS doing the so called ride-through. Here, the same strategy implemented on the real WTGS is used in the simulation to ensure the correlation between the simulation and the real test.

The strategy consists in substituting the torque and stator reactive power control current reference signals computed from (24) by a pair of constant values. According to the quasi-decoupled active and reactive power control obtained from the stator flux *qd* orientation, giving a 0 as the i_{rd} reference signal during the dip, suppresses the generator's torque and the active power flowing through the rotor windings thus minimizing the power through the rotor-side converter and the rise of the DC bus voltage. Also, giving a non-zero value as the i_{rq} reference signal allows generating reactive power to the grid which may be desirable during voltage dips to rise the grid's voltage.

As the grid voltage reaches its nominal value, the constant current reference signals are substituted again by the ones computed from (24). The torque reference is kept constant for a few seconds and then switched back to the output of the speed control torque reference signal.

4.1. Controller response

In this section a series of graphs of the evolution of some relevant internal variables of the model are presented which show the proper behavior of the different WTGS control loops. Note that this variables were not measured on the real test thus no comparison with the actual system evolution is shown, proper comparison between simulation and experimental measurements will be presented for the MV variables later.

Fig. 12 shows rotor current evolution and its reference values. i_{rd} current reference value is kept constant for one second after the rise of the voltage and as said before, the control over the current is lost during the crow bar connection. The voltage output actuation signal can be seen in Fig. 13. It can be seen that the *d* component does not remain constant despite the constant value of the torque reference due to the linearization state feedback which depends on the mechanical speed. Fig. 14 shows the stator reactive power and generator torque obtained and its reference signals. Notice that torque reference from the speed control is ignored during the voltage dip. The evolution of the angular speed of the generator can be seen in Fig. 15, the speed during the voltage dip is increased due to the absence of generator torque.

The grid-side converter control DC bus voltage and reactive power reference inputs are kept constant despite the voltage dip. The currents through the converter and its reference values can be seen in Fig. 16. The voltages applied by the converter on the AC side can be seen in Fig. 17. The evolution of the DC bus voltage can be seen in Fig. 18.

4.2. Comparison with experimental results

In this section a comparison between the simulation results and the simulated evolution of the system is presented.

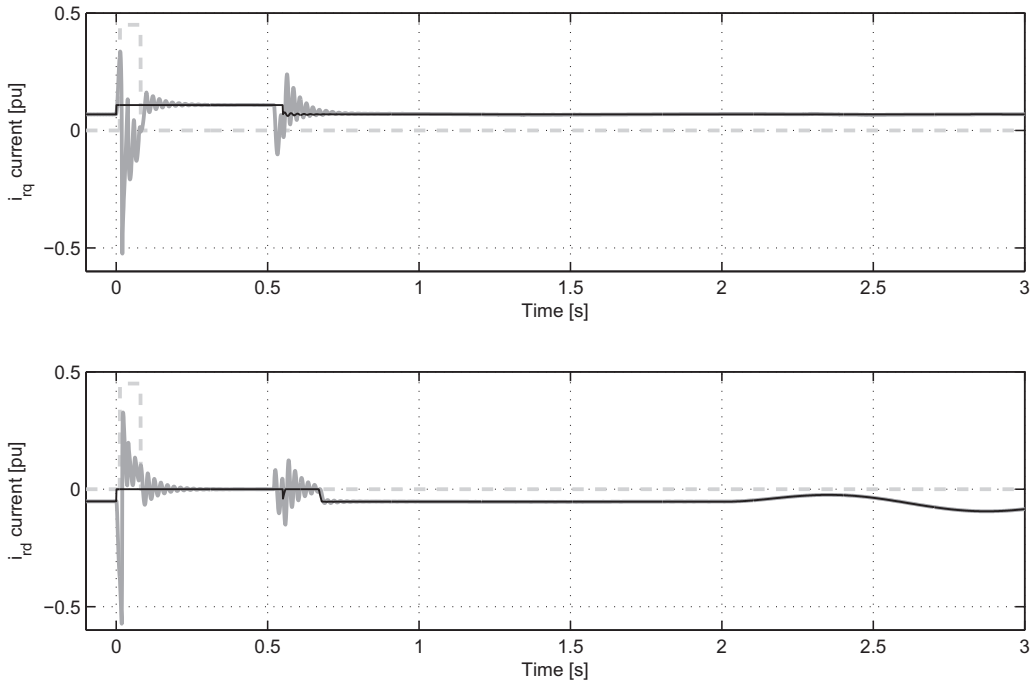

Fig. 12. Generator rotor currents in the stator flux *qd* frame. Continuous black line – reference value; continuous grey line – actual value; grey dashed line – crow bar connection state.

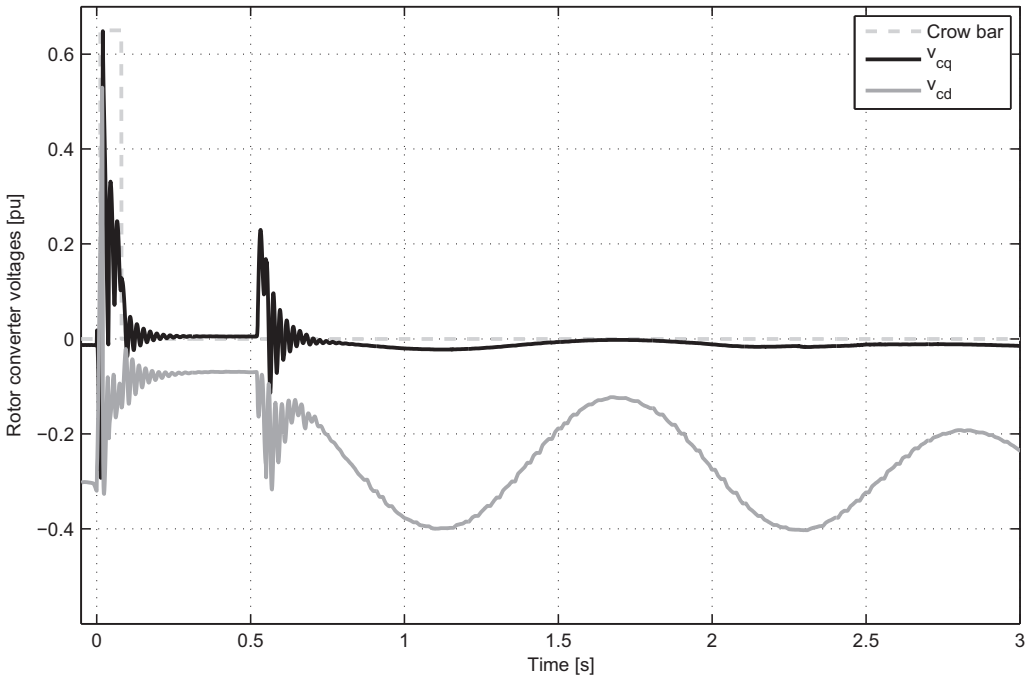

Fig. 13. Rotor-side converter AC output voltages in the stator flux *qd* reference frame during the voltage dip.

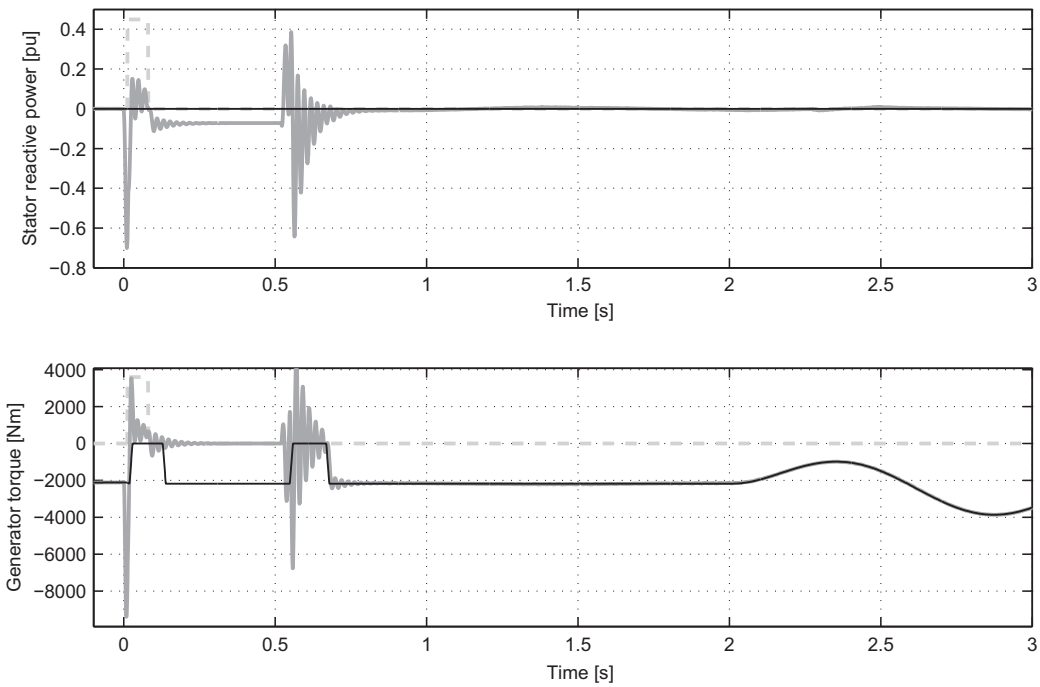

Fig. 14. Stator reactive power and generator torque during the voltage dip. Continuous grey line – output values; continuous black line – reference value; grey dashed line – crow bar connection state.

Fig. 19 shows the evolution of the active and reactive power output of the TR1 transformer on the MV-side. The comparison of the evolution of the RMS values of the currents on the MV-side of the transformer can also be seen on Fig. 20.

The comparison shows that the variables obtained from the simulated model and the measured evolution on the real system are very close despite the real system show a slightly slower evolution of the reactive power at the end of the gap. As the

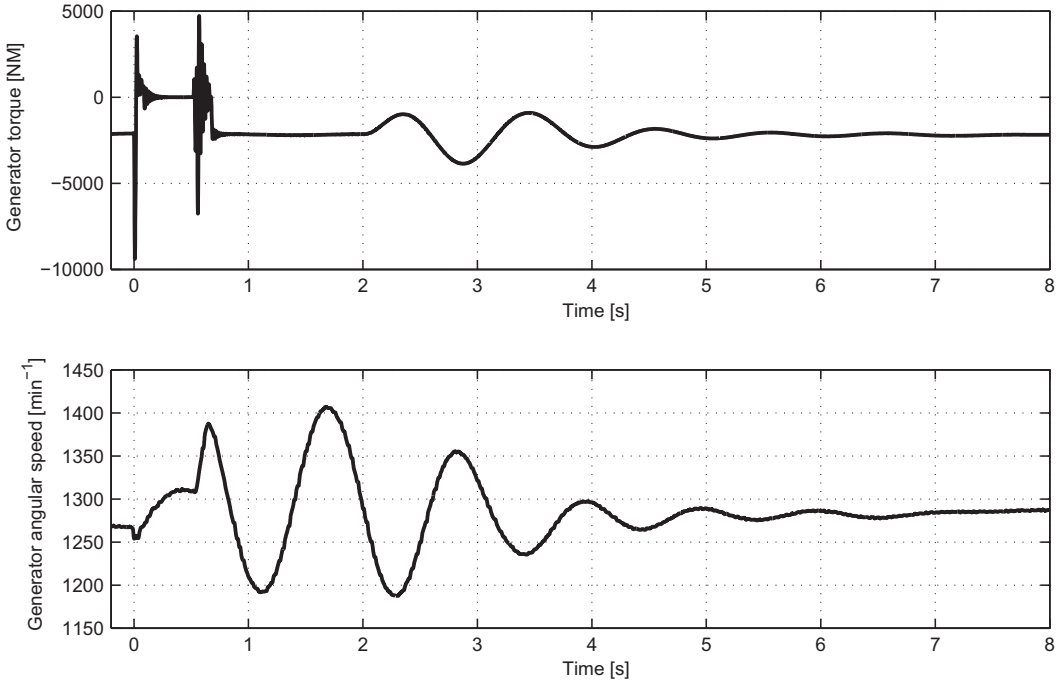

Fig. 15. Generator torque and angular speed.

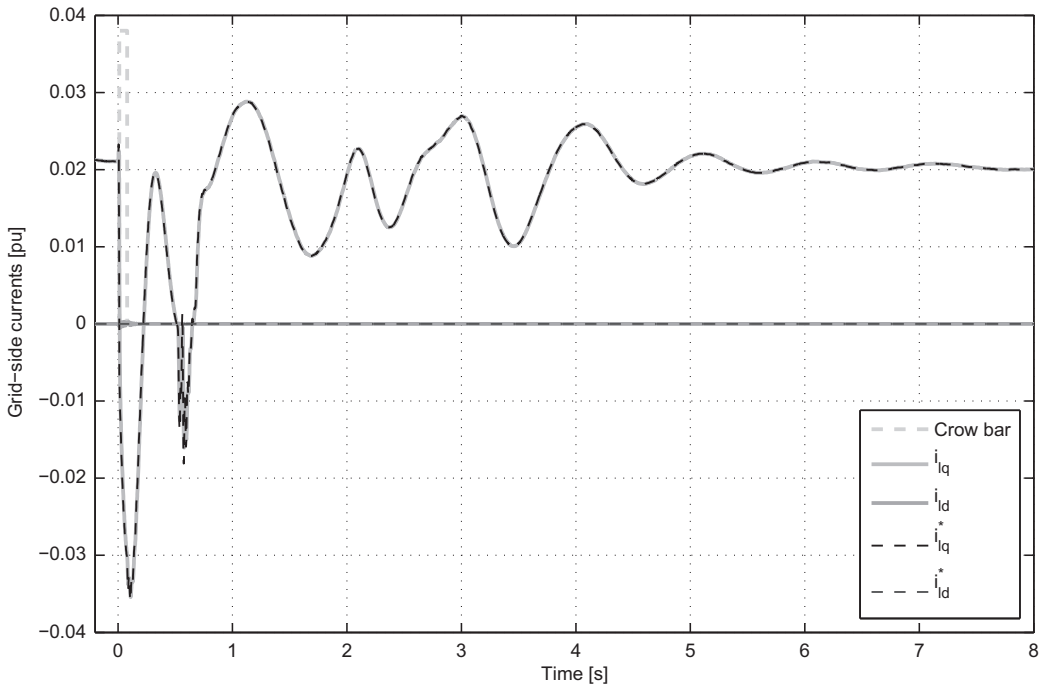

Fig. 16. Grid-side converter AC output currents in the stator flux *qd* reference frame during the voltage dip.

measurements were made on the MV-side of the TR1 transformer, the close resemblance of the active power evolution suggest that the neglection of the TR1 transformer magnetizing inductance transients and its non-linear behavior may be the cause of these differences. Nonlinear dynamical models of transformers can be found in the literature which can be adapted

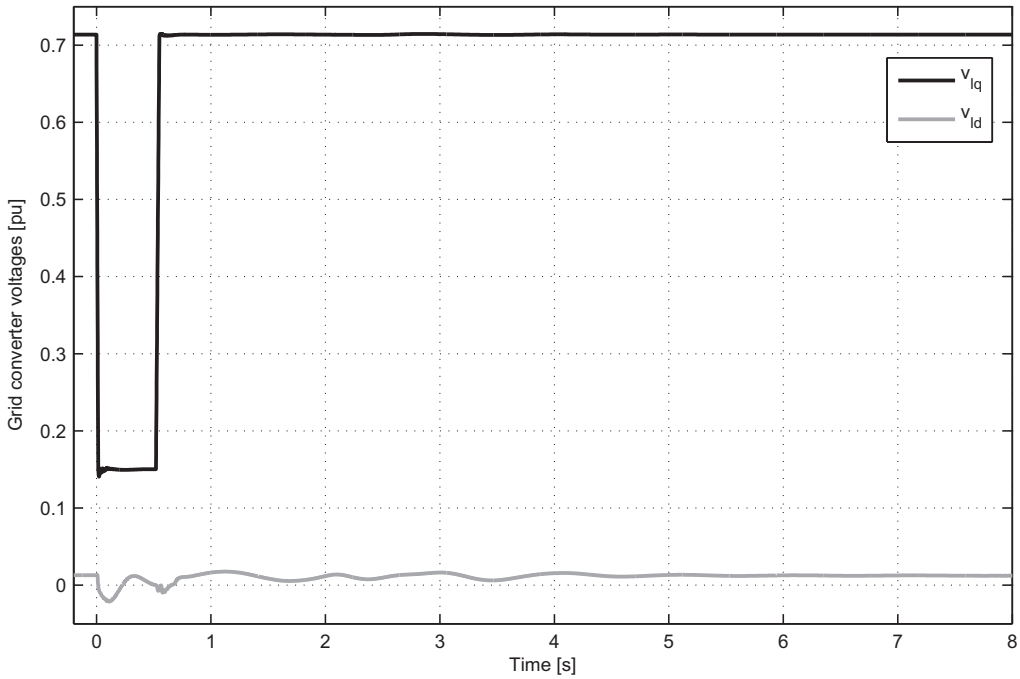

Fig. 17. Grid-side converter AC output voltages in the stator flux *qd* reference frame during the voltage dip.

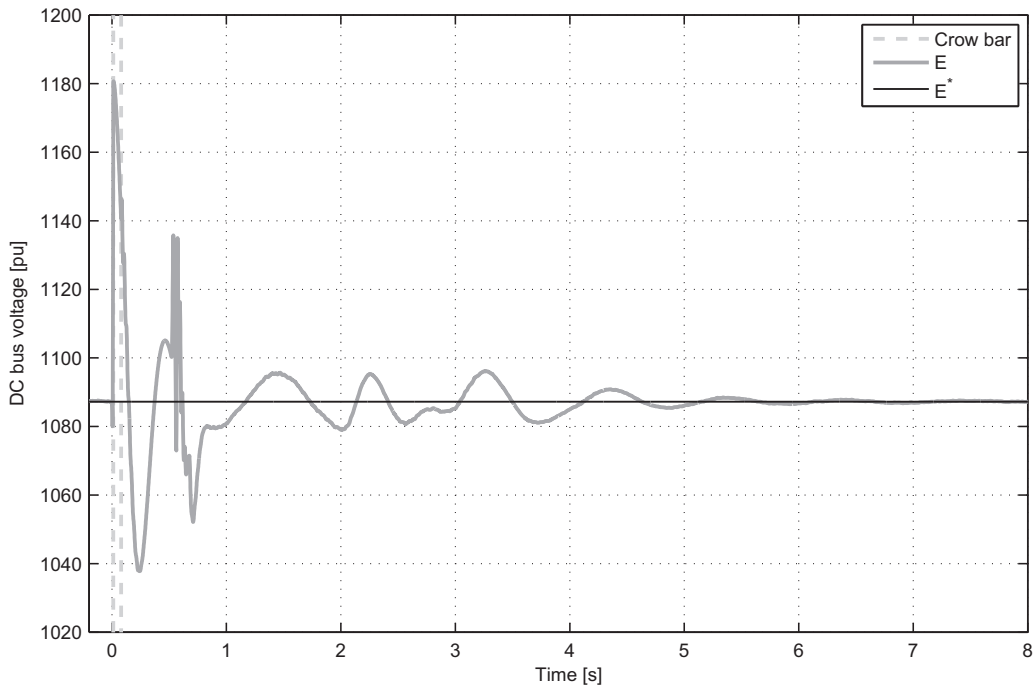

Fig. 18. DC bus voltage during the voltage dip.

from experimental data from transformer tests [26] and could be added to the model to improve its accuracy. Unfortunately, to adapt the model, measures from both sides of the transformer, which are not available here, would be necessary to do it.

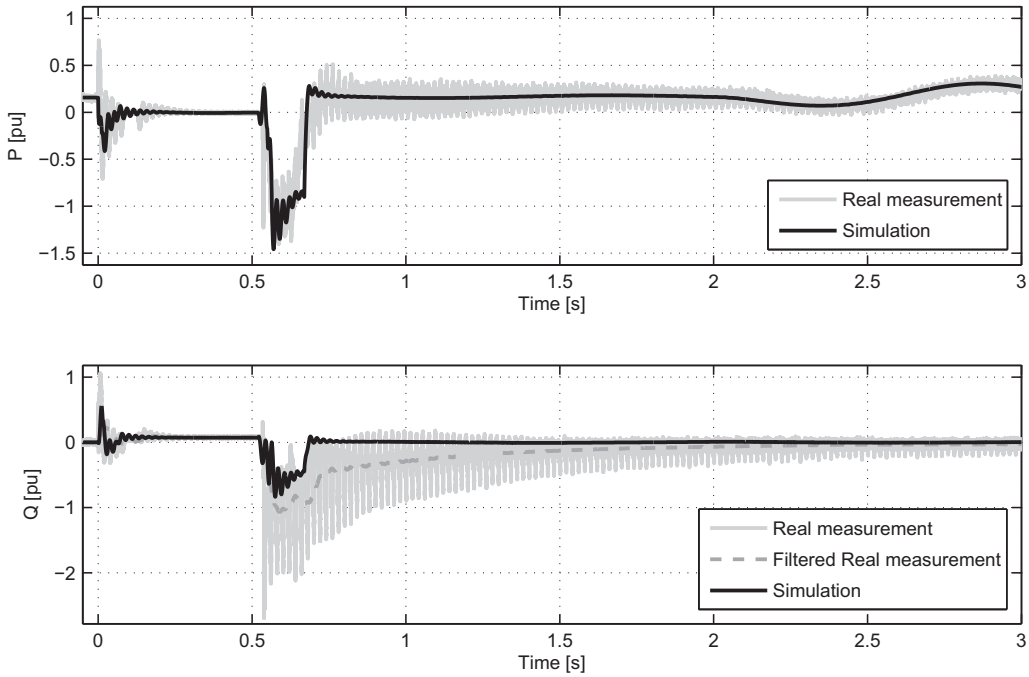

Fig. 19. Active and reactive power output of the SGTV measured on the MV-side of the TR1 transformer.

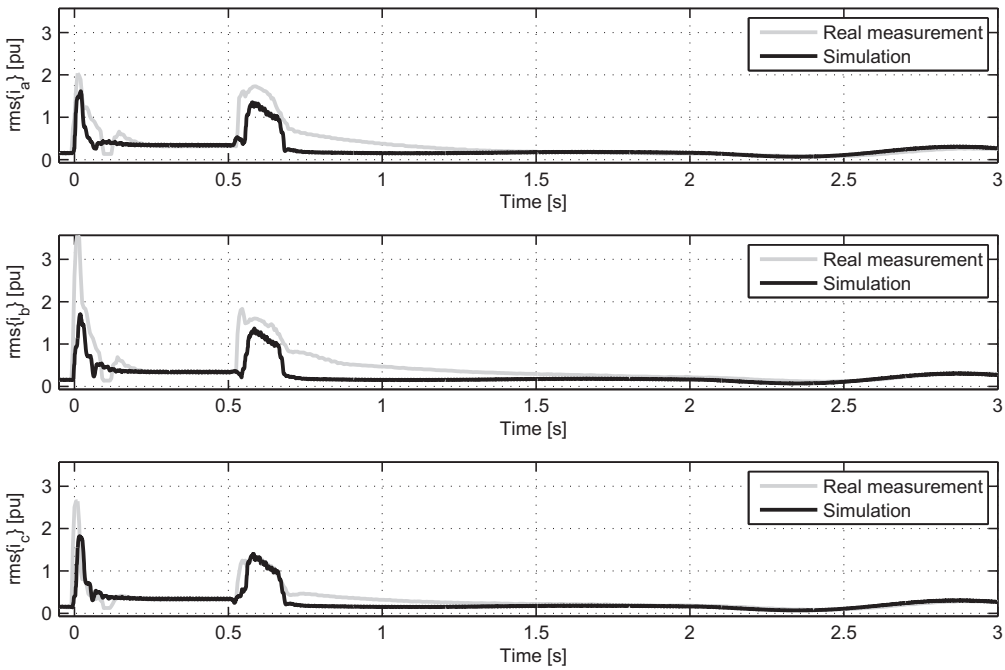

Fig. 20. RMS value of the *abc* currents of the MV-side of the TR1 transformer.

5. Conclusions

The paper has presented a model for a wind turbine generation system based on a doubly fed induction generator. A detailed modeling of the mechanical dynamics, the wind turbine electrical system, the converter and the electrical grid has been presented and the design of the control loops for each subsystem has been discussed. Special attention is dedicated to ride-through capability of the system, studying the behaviour of the model under voltage dip condition. The results are

compared to experimental data extracted from real voltage sags provoked to wind turbines, the ressemblance between the simulated evolution and the experimental data suggest the model is able to produce useful results for wind turbine behavior studies.

Acknowledgements

This work was supported by the *Ministerio de Ciencia e Innovación* under the project ENE2009-08555.

References

[1] Z. Lubosny, Wind Turbine Operation in Electric Power Systems, Springer, 2003.
[2] Yazhou Lei, A. Mullane, G. Lightbody, R. Yacamini, Modeling of the wind turbine with a doubly fed induction generator for grid integration studies, IEEE Transactions on Energy Conversion 21 (1) (2006) 257–264.
[3] T. Petru, T. Thiringer, Modeling of wind turbines for power system studies, IEEE Transactions on Power Systems 17 (4) (2002) 1132–1139.
[4] P. Ledesma, J. Usaola, Doubly fed induction generator model for transient stability analysis, IEEE Transactions on Energy Conversion 20 (2) (2005) 388–397.
[5] Anca D. Hansen, Gabriele Michalke, Fault ride-through capability of DFIG wind turbines, Renewable Energy 32 (9) (2007) 1594–1610.
[6] J. Morren, S.W.H. de Haan, Ridethrough of wind turbines with doubly-fed induction generator during a voltage dip, IEEE Transactions on Energy Conversion 20 (2) (2005) 435–441.
[7] A. Petersson, S. Lundberg, T. Thiringer, A DFIG wind turbine ride-through system, influence on the energy production, Wind Energy 8 (3) (2005) 251–263.
[8] S. Seman, J. Niiranen, A. Arkkio, Ride-through analysis of doubly fed induction wind-power generator under unsymmetrical network disturbance, IEEE Transactions on Power Systems 21 (4) (2006) 1782–1789.
[9] T.K.A. Brekken, N. Mohan, Control of a doubly fed induction wind generator under unbalanced grid voltage conditions, IEEE Transaction on Energy Conversion 22 (1) (2007) 129–135.
[10] Dawei Xiang, Li Ran, P.J. Tavner, S. Yang, Control of a doubly fed induction generator in a wind turbine during grid fault ride-through, IEEE Transactions on Energy Conversion 21 (3) (2006) 652–662.
[11] R. Pena, J.C.J.C. Clare, G.M. Asher, Doubly fed induction generator using back-to-back PWM convertersand its application to variable-speed wind-energy generation, IEE Proceedings Electric Power Applications 143 (3) (1996) 231–241.
[12] Badrul H. Chowdhury, Srinivas Chellapilla, Double-fed induction generator control for variable speed wind power generation, Electric Power Systems Research 76 (9–10) (2006) 786–800.
[13] Paul-Etienne Vidal, Maria Pietrzak-David, Frantois Bonnet, Mixed control strategy of a doubly fed induction machine, Electrical Engineering (Archiv fur Elektrotechnik) 90 (5) (2008) 337–346.
[14] Sergei Peresada, Andrea Tilli, Alberto Tonielli, Power control of a doubly fed induction machine via output feedback, Control Engineering Practice 12 (1) (2004) 41–57.
[15] S. Peresada, A. Tilli, A. Tonielli, Indirect stator flux-oriented output feedback control of a doubly fed induction machine, IEEE Transactions on Control Systems Technology 11 (6) (2003) 875–888.
[16] R. Cardenas, R. Pena, J. Proboste, G. Asher, J. Clare, MRAS observer for sensorless control of standalone doubly fed induction generators, IEEE Transaction on Energy Conversion 20 (4) (2005) 710–718.
[17] Anca D. Hansen, Poul Sorensen, Florin Iov, Frede Blaabjerg, Centralised power control of wind farm with doubly fed induction generators, Renewable Energy 31 (7) (2005) 935–951.
[18] J.L. Rodrfguez-Amenedo, S. Arnaltes, M.A. Rodrfguez, Operation and coordinated control of fixed and variable speed wind farms, Renewable Energy (2007).
[19] S. Heier, Grid Integration of Wind Energy Conversion Systems, John Wiley and Sons, 1998.
[20] J.G. Slootweg, Reduced-order modelling of wind turbines, in: Wind Power in Power Systems, Wiley, 2005, pp. 555–585.
[21] Hans A. Panofsky, John A. Dutton, Atmospheric Turbulence, Wiley-Interscienc, 1984.
[22] M. Shinozuka, C.-M. Jan, Digital simulation of random processes and its applications, Journal of Sound and vibration 25 (1) (1972) 111–128.
[23] Jamal A. Baroudi, Venkata Dinavahi, Andrew M. Knight, A review of power converter topologies for wind generators, Renewable Energy 32 (14) (2007) 2369–2385.
[24] L. Harnefors, H.-P. Nee, Model-based current control of ac machines using the internal model control method, IEEE Transactions on Industry Applications 34 (1) (1998) 133–141.
[25] Tingshu Hu, Zongli Lin, Control Systems with Actuator Saturation Analysis and Design, BirkhSuser, 2001.
[26] J.H. Chan, A. Vladimirescu, X.-C. Gao, P. Liebmann, J. Valainis, Nonlinear transformer model for circuit simulation, IEEE Transactions on Computer-Aided Design of Integrated Circuits and Systems 10 (4) (1991) 476–482.